INTERNATIONAL CIVIL ENGINEERING AND ARCHITECTURE CONFERENCE 2019
ICEARC'19
17-20 APRIL 2019 TRABZON / TURKEY
Karadeniz Technical University

THE WARPING EFFECT ON THE STRUCTURAL RESPONSE OF SANDWICH EXACT HELICAL RODS

Umit N. Aribas [1], Merve Ermis [2], Akif Kutlu [2], Nihal Eratli [2], Mehmet H. Omurtag [2]

[1] *Istanbul Okan University, Department of Civil Engineering, Istanbul, Turkey*
[2] *Istanbul Technical University, Department of Civil Engineering, Istanbul, Turkey*

Abstract

The objective of this research is to investigate the influence of cross-sectional warping on the precision of the forces/moments of exact conical helices with sandwich rectangular cross-sections. The exact axial geometries of conical helices are derived over both Archimedean and logarithmic planar curves. Since the curved structural elements generally fall under the influence of torque, the determination of cross-sectional warping included torsional rigidity of composite non-circular cross-sections has a great importance. The analyses are performed using the mixed finite element method based on Timoshenko beam theory. The cross-sectional warping included torsional rigidity of a sandwich rectangular section is determined using a numerical method and the result is used in the mixed finite element formulation. Two-noded curved finite elements are used with 12 degrees of freedom at per node (three translations, three rotations, two shear forces, one axial force, two bending moments and one torque). The shear influence is considered in the analysis. The exact conical helix has fixed boundary conditions at both ends and it is under the influence of a uniformly distributed load. The necessary number of finite elements is determined by a convergence analysis for the reactions at the supports of the exact conical helix. The results are compared with the results obtained using displacement type elements of SAP2000. As a benchmark example, a parametric analysis is performed for the cross-sectional warping included maximum absolute forces/moments along the length of the exact conical helix over Archimedean and logarithmic planar curves. In order to emphasize the importance of the research, the results of the present FE formulation are compared with the FE results obtained using the conventional torsional rigidity, which disregards the warping effect.

Keywords: Sandwich; Warping; Torsional rigidity; Static analysis; Finite element

1. Introduction

The design of composite structures yields stiffer/lighter cross-sections compare to traditional materials. Thus, the composite structural elements have widespread application fields such as aerospace, biomedicine, marine, mechanical/civil engineering industries. The design of composite straight/planar curved rods attracted the interest of many researches due to their above mentioned advantages (Abramovich and Livshits 1994; Aguiar et al. 2012; Aydogdu 2005; Babuska et al. 2018; Bhimaraddi and Chandrashekhara 1991; Carpentieri et al. 2015; Hu et al. 1985; Jun et al. 2008; Kapania and Raciti 1989; Kennedy et al. 2011; Khdeir and Reddy 1997; Krishnaswamy et al. 1992; Nguyen et al., 2018, 2017; Vo and Thai 2012; Yan et al. 2017). Although the static and dynamic analyses of straight/planar curved rods are investigated intensively in the literature, the researches for the design of composite helices are quite rare (Çalım 2009; Temel et al. 2005; Yıldırım 1999; Yıldırım and Sancaktar 2000; Yousefi and Rastgoo 2011; Yu and Hao 2013). The determination of warping included torsional rigidity has a great importance since the applied forces cause torque for the curved structural elements. There are some studies in the field of warping included torsional rigidity of orthotropic composite sections in literature (Barretta 2012; Darılmaz et al. 2018; El Fatmi and Ghazouani 2011; El Fatmi and Zenzri 2004; Jog and Mokashi 2014; Nouri and Gay 1994; Savoia and Tullini 1993; Swanson 1998). However, regarding to the authors' best knowledge, a research in the field of cross-sectional warping included forces/moments of exact conical helices does not exist.

In this research, considering the cross-sectional warping, the absolute maximum forces/moments along the axis of exact conical helices over Archimedean and logarithmic planar curves are investigated. In order to emphasize the importance of the warping of cross-section, warping included results are compared to the results obtained using

the conventional method, which disregards the warping. The exact conical helix geometry is derived over associated plane curves (Ermis and Omurtag 2017). The analyses are performed using the mixed finite element method. The two-noded curved finite elements have 24 nodal variables in total. The cross-sectional warping included torsional rigidity of sandwich rectangular cross-section is determined using the numerical method given in Aribas et al. (2019) and it is used in the mixed finite element formulation. The influence of cross-sectional warping on the precision of maximum forces/moments along the axis of exact conical helices are investigated. A parametric analysis is performed for the taper ratio and the number of the active turns.

2. Formulation

2.1. The constitutive equations of orthotropic composites

The generalized Hooke's law of an orthotropic material is defined as $\boldsymbol{\sigma} = \mathbf{E}\boldsymbol{\varepsilon}$, where $\mathbf{E}$ is the elasticity matrix of the orthotropic body and $\boldsymbol{\sigma}$ and $\boldsymbol{\varepsilon}$ are the stress and strain tensors, respectively. The laminated composites made of layers with various principle material direction orientations may provide better stiffness and strength. Thus, the transformation of the principle axis of orthotropic layers around *b*-axis of the laminate is introduced (Jones 1999),

$$\bar{\boldsymbol{\sigma}} = \mathbf{T}^{-1}\mathbf{E}\,\mathbf{T}^{-\mathrm{T}}\;\bar{\boldsymbol{\varepsilon}} = \bar{\mathbf{E}}\,\bar{\boldsymbol{\varepsilon}} \tag{2.1}$$

where, the transformation matrix is $\mathbf{T}$ and transformed elasticity matrix, stress and strain vectors are $\bar{\mathbf{E}}$, $\bar{\boldsymbol{\sigma}}$ and $\bar{\boldsymbol{\varepsilon}}$, respectively. The reduction of the constitutive equations of orthotropic body under the assumptions of classical rod theory $\sigma_n = \sigma_b = \tau_{nb} = 0$ yields the constitutive equations of a single orthotropic layer (Yıldırım 1999), where *t*, *n* and *b* are the Frenet coordinates. Letting the transformed-reduced stress vector $\bar{\boldsymbol{\sigma}}_L = \{\sigma_t \quad \tau_{bt} \quad \tau_{tn}\}_L^T$ and the transformed-reduced strain tensor $\bar{\boldsymbol{\varepsilon}}_L = \{\varepsilon_t \quad \gamma_{bt} \quad \gamma_{tn}\}_L^T$, the constitutive equation of a layer is defined as $\bar{\boldsymbol{\sigma}}_L = \bar{\boldsymbol{\beta}}_L\,\bar{\boldsymbol{\varepsilon}}_L$ where, $\bar{\boldsymbol{\beta}}_L$ is a matrix of orthotropic material constants and L is the number of layers. The displacements at the beam continuum are $u_t^* = u_t + b\Omega_n - n\Omega_b$, $u_n^* = u_n - b\Omega_t$ and $u_b^* = u_b + n\Omega_t$ (Yousefi and Rastgoo 2011), where u_t, u_n and u_b are displacements on the axis and Ω_t, Ω_n and Ω_b are the rotations of the section about the Frenet coordinates. The constitutive equations of a single layer over kinematic relations yield (Bhimaraddi and Chandrashekhara 1991),

$$\begin{Bmatrix}\sigma_t\\ \tau_{bt}\\ \tau_{tn}\end{Bmatrix}_L = \bar{\boldsymbol{\beta}}_L \left\{ \begin{Bmatrix} u_{t,t} \\ u_{t,b} + u_{b,t} \\ u_{t,n} + u_{n,t} \end{Bmatrix} + b \begin{Bmatrix} \Omega_{n,t} \\ 0 \\ -\Omega_{t,t} \end{Bmatrix} + n \begin{Bmatrix} -\Omega_{b,t} \\ \Omega_{t,t} \\ 0 \end{Bmatrix} \right\}_L \tag{2.2}$$

where, the number of the layer is $L = 1,...,N$ and the total number of layers is N. The commas in the subscripts denote the partial derivations. The analytical integration of stresses through the thickness of cross-section indicates the forces T_t, T_n, T_b and moments M_t, M_n, M_b on the cross-section,

$$\begin{aligned}
T_t &= \sum_{L=1}^{N} \int_{-0.5n_L}^{0.5n_L} \int_{b_{L-1}}^{b_L} \sigma_t \mathrm{d}b\;\mathrm{d}n \\
M_t &= \sum_{L=1}^{N} -\int_{-0.5n_L}^{0.5n_L} \int_{b_{L-1}}^{b_L} b\,\tau_{tn}\mathrm{d}b\;\mathrm{d}n + \int_{b_{L-1}}^{b_L} \int_{-0.5n_L}^{0.5n_L} n\,\tau_{tb}\mathrm{d}n\;\mathrm{d}b \\
T_n &= \sum_{L=1}^{N} \int_{-0.5n_L}^{0.5n_L} \int_{b_{L-1}}^{b_L} \tau_{tn}\mathrm{d}b\;\mathrm{d}n \quad ; \quad M_n = \sum_{L=1}^{N} \int_{-0.5n_L}^{0.5n_L} \int_{b_{L-1}}^{b_L} b\sigma_t \mathrm{d}b\;\mathrm{d}n \\
T_b &= \sum_{L=1}^{N} \int_{-0.5n_L}^{0.5n_L} \int_{b_{L-1}}^{b_L} \tau_{bt}\mathrm{d}b\;\mathrm{d}n \quad ; \quad M_b = -\sum_{L=1}^{N} \left(\int_{b_{L-1}}^{b_L} \left(\int_{-0.5n_L}^{0.5n_L} n\sigma_t \mathrm{d}n \right) \mathrm{d}b \right)
\end{aligned} \tag{2.3}$$

where, the width of the layer is n_L, the directed distances to the bottom and top of the L^{th} layer are b_L and b_{L-1} where *b* indicates positive upward. By means of the Eqn. (2.3), the constitutive equations of the composite section in a matrix form becomes,

$$\begin{Bmatrix} u_{t,t} \\ u_{t,n}+u_{n,t} \\ u_{t,b}+u_{b,t} \\ \Omega_{t,t} \\ \Omega_{n,t} \\ \Omega_{b,t} \end{Bmatrix} = \begin{bmatrix} \mathbf{C}_m & \mathbf{C}_{mf} \\ \mathbf{C}_{fm} & \mathbf{C}_f \end{bmatrix} \begin{Bmatrix} T_t \\ T_n \\ T_b \\ M_t \\ M_n \\ M_b \end{Bmatrix} \tag{2.4}$$

where, $\mathbf{C}_m$, $\mathbf{C}_{mf}$, $\mathbf{C}_{fm}$, $\mathbf{C}_f$ are the compliance matrices and $\mathbf{C}_{mf}$, $\mathbf{C}_{fm}$ are the coupling matrices. The cross-sectional warping included torsional rigidity of composite non-circular sections is determined using the numerical method given in Aribas et al. (2019). The results are used in the mixed finite element formulation.

2.2. Functional and mixed finite element formulation

The exact axial geometry of conical helix over Archimedean and logarithmic planar curves is derived using the function given in Ermis and Omurtag (2017). The field equations of an isotropic curved Timoshenko rod (Omurtag and Aköz 1992) are extended to laminated composites,

$$\begin{matrix} -\mathbf{T}_{,s}-\mathbf{q}=0 \\ -\mathbf{M}_{,s}-\mathbf{t}\times\mathbf{T}-\mathbf{m}=0 \end{matrix} \quad ; \quad \begin{matrix} -\mathbf{C}_{fm}\mathbf{T}-\mathbf{C}_f\mathbf{M}+\boldsymbol{\Omega}_{,s}=0 \\ -\mathbf{C}_m\mathbf{T}-\mathbf{C}_{mf}\mathbf{M}+\mathbf{u}_{,s}+\mathbf{t}\times\boldsymbol{\Omega}=0 \end{matrix} \tag{2.5}$$

where, the distributed external force and moment vectors are $\mathbf{q}$ and $\mathbf{m}$, respectively. The force and moment vectors are $\mathbf{T}$ and $\mathbf{M}$, respectively. The displacement and cross-sectional rotation vectors are $\mathbf{u}$ and $\boldsymbol{\Omega}$, respectively. The functional is derived based on the Gâteaux differential and the potential operator concept (Oden and Reddy 2012; Omurtag and Aköz 1994),

$$\begin{aligned} I(\mathrm{y}) = & -\left[\mathbf{T}_{,s},\mathbf{u}\right]-\left[\mathbf{M}_{,s},\boldsymbol{\Omega}\right]+\left[\mathbf{t}\times\boldsymbol{\Omega},\mathbf{T}\right] \\ & -\tfrac{1}{2}\left\{\left[\left(\mathbf{C}_m\right)\mathbf{T},\mathbf{T}\right]+\left[\left(\mathbf{C}_{mf}\right)\mathbf{M},\mathbf{T}\right]+\left[\left(\mathbf{C}_{fm}\right)\mathbf{M},\mathbf{T}\right]+\left[\left(\mathbf{C}_f\right)\mathbf{M},\mathbf{M}\right]\right\} \\ & +\left[\mathbf{T},\hat{\mathbf{u}}\right]_\varepsilon+\left[\mathbf{M},\hat{\boldsymbol{\Omega}}\right]_\varepsilon+\left[\left(\mathbf{T}-\hat{\mathbf{T}}\right),\mathbf{u}\right]_\sigma+\left[\left(\mathbf{M}-\hat{\mathbf{M}}\right),\boldsymbol{\Omega}\right]_\sigma \\ & -\left[\mathbf{q},\mathbf{u}\right]-\left[\mathbf{m},\boldsymbol{\Omega}\right] \end{aligned} \tag{2.6}$$

The linear interpolation functions are used. The two-noded curved finite elements, which have 24 degrees of freedom in total, are derived over the exact functions of curvature, torsion and arc length of helix geometry. Shear influence is considered and the shear correction factor is 5/6.

3. Numerical Example

A parametric study is performed in order to determine the influence of cross-sectional warping on the precision of the results (especially on forces/moments) along the axis of exact conical helix over Archimedean and logarithmic planar curves. The cross-sectional warping included absolute maximum forces/moments are compared to the absolute maximum forces/moments obtained using the conventional method, which disregards the warping effect. The function given in Ermis and Omurtag (2017) is used for the exact axial geometry of conical helix. The both ends of the exact conical helix are fixed. The parametric analysis is performed by keeping the maximum radius constant $R_{\max}=100\,\mathrm{mm}$ and setting the taper ratio to $\xi = R_{\min}/R_{\max}$ 0.8 , 0.6 and 0.4. For each taper ratio, the number of the active turns is set to $n=$ 2 , 4 and 6. The exact axial geometry of conical helix is generated using a constant pitch angle $\alpha=5^\circ$. There is a uniformly distributed vertical load 0.25N/m along the axis of the exact conical helix. The maximum influence of cross-sectional warping on torsional rigidity of sandwich sections is obtained for $\lambda=b/h$ 0.3 and $h_{\mathrm{Core}}/h\cong 0.7$ in the case of $h>b$ within the investigations in Aribas et al. (2019) where b is the width and h is the thickness of the laminate. Thus, the width, thickness of the laminate and the thickness of the core are $b=3\,\mathrm{mm}$, $h=10\,\mathrm{mm}$ and $h_{\mathrm{core}}=7\,\mathrm{mm}$, respectively. The core is made of magnesium and the faces are steel. The Young's modulus, shear modulus and Poisson's ratio of magnesium are 45.0 GPa, 17.442 GPa and 0.29, respectively. The Young's modulus, shear modulus and Poisson ratio of steel are 210.0 GPa, 80.769 GPa and 0.3, respectively. The warping included average torsional rigidity GI_t of the sandwich cross-section is 1.85Nm^2. The convergence analysis for the given exact conical helices is performed in Aribas et al. (2019) and it is stated that the results obtained using 600 mixed type curved elements are in an excellent agreement with the results of displacement type straight elements of SAP2000. In this example, the cross-sectional warping included maximum absolute forces/moments along the axis of exact conical helix are compared to the maximum absolute results obtained using conventional method which disregards the warping (Tables 1 and 2).

Table 1. The warping included maximum absolute forces $|T_t|,|T_n^-|,|T_b|$ and moments $|M_t|,|M_n^-|,|M_b|$ along the axis of exact conical helix over Archimedean planar curve compare to the maximum forces $|T_t|,|T_n|,|T_b|$ and moments $|M_t|,|M_n|,|M_b|$, which disregard warping. The units are N for forces and Nm for moments.

	$n=2$			$n=4$			$n=6$		
	$\xi=0.8$	$\xi=0.6$	$\xi=0.4$	$\xi=0.8$	$\xi=0.6$	$\xi=0.4$	$\xi=0.8$	$\xi=0.6$	$\xi=0.4$
T_t	0.0183	0.0195	0.0205	0.0326	0.0359	0.0383	0.0458	0.0496	0.0520
T_t	0.0123	0.0124	0.0121	0.0268	0.0269	0.0262	0.0411	0.0408	0.0396
T_n	0.0072	0.0085	0.0100	0.0074	0.0115	0.0153	0.0069	0.0121	0.0168
T_n	0.0007	0.0010	0.0012	0.0012	0.0021	0.0028	0.0016	0.0030	0.0040
T_b	0.1486	0.1394	0.1285	0.3012	0.2865	0.2671	0.4533	0.4325	0.4045
T_b	0.1495	0.1413	0.1309	0.3024	0.2888	0.2703	0.4546	0.4350	0.4079
M_t	0.0127	0.0101	0.0079	0.0257	0.0208	0.0163	0.0388	0.0314	0.0247
M_t	0.0129	0.0102	0.0079	0.0261	0.0210	0.0165	0.0392	0.0316	0.0249
M_n	0.0067	0.0060	0.0054	0.0071	0.0068	0.0063	0.0075	0.0074	0.0071
M_n	0.0058	0.0052	0.0047	0.0059	0.0054	0.0049	0.0061	0.0057	0.0052
M_b	0.0013	0.0012	0.0010	0.0025	0.0022	0.0022	0.0036	0.0032	0.0030
M_b	0.0010	0.0007	0.0003	0.0021	0.0015	0.0012	0.0032	0.0025	0.0021

Table 2. The warping included maximum absolute forces $|T_t|,|T_n^-|,|T_b|$ and moments $|M_t|,|M_n^-|,|M_b|$ along the axis of exact conical helix over logarithmic planar curve compare to the maximum forces $|T_t|,|T_n|,|T_b|$ and moments $|M_t|,|M_n|,|M_b|$, which disregard warping. The units are N for forces and Nm for moments.

	$n=2$			$n=4$			$n=6$		
	$\xi=0.8$	$\xi=0.6$	$\xi=0.4$	$\xi=0.8$	$\xi=0.6$	$\xi=0.4$	$\xi=0.8$	$\xi=0.6$	$\xi=0.4$
T_t	0.0183	0.0193	0.0195	0.0325	0.0355	0.0369	0.0457	0.0490	0.0502
T_t	0.0123	0.0122	0.0113	0.0267	0.0265	0.0248	0.0409	0.0402	0.0380
T_n	0.0072	0.0085	0.0097	0.0074	0.0115	0.0151	0.0070	0.0121	0.0167
T_n	0.0007	0.0010	0.0011	0.0012	0.0021	0.0028	0.0016	0.0030	0.0040
T_b	0.1480	0.1369	0.1215	0.3001	0.2817	0.2545	0.4516	0.4255	0.3861
T_b	0.1490	0.1387	0.1240	0.3013	0.2841	0.2578	0.4530	0.4281	0.3896
M_t	0.0126	0.0098	0.0069	0.0256	0.0201	0.0146	0.0386	0.0305	0.0222
M_t	0.0128	0.0098	0.0069	0.0259	0.0203	0.0147	0.0390	0.0307	0.0223
M_n	0.0067	0.0060	0.0053	0.0071	0.0068	0.0062	0.0075	0.0074	0.0070
M_n	0.0058	0.0053	0.0046	0.0059	0.0055	0.0050	0.0061	0.0057	0.0053
M_b	0.0013	0.0011	0.0009	0.0025	0.0021	0.0020	0.0036	0.0031	0.0028
M_b	0.0010	0.0007	0.0003	0.0021	0.0014	0.0010	0.0032	0.0024	0.0018

The cross-sectional warping included maximum absolute forces $|T_t|$, $|T_n|$ and moments $|M_n|$, $|M_b|$ of exact conical helices over both Archimedean and logarithmic planar curves are greater than their corresponding results obtained disregarding the warping effect (Tables 1 and 2). The force $|T_t|$ of both exact conical helices increases as the taper ratio ξ decreases. However, the force obtained using the conventional method $|T_t|$ of exact conical helix over logarithmic planar curve decreases as ξ decreases. The forces $|T_t|$ and $|T_t|$ of both exact conical helices increases as the number of the active turns n increases. The forces $|T_n|$ and $|T_n|$ of both exact conical helices

increases as ξ decreases. The moments $|M_n|$, $|M_b|$, $|M_n|$ and $|M_b|$ of both exact conical helices decreases as ξ or n decreases.

The ratio of the cross-sectional warping included maximum absolute results of both exact conical helices to the corresponding maximum absolute results obtained using the conventional method is denoted by β. The ratio $\beta > 1$ for the force T_t increases as the taper ratio ξ decreases (Figures 1a-1b) or the number of active turns n decreases (Figures 1c-1d). The ratio $\beta > 1$ for the force T_n increases as n decreases (Figures 2a-2b). The maximum ratio $\beta \cong 9.68$ is obtained for the force T_n in the case of $\xi =$ 0.8 and $n = 2$ compare to the ratios β of other forces/moments within all cases. The ratio $\beta < 1$ for the force T_b decreases as ξ decreases (Figures 3a-3b) or n decreases (Figures 3c-3d). The minimum ratio $\beta \cong 0.98$ is obtained for the force T_b in the case of $\xi =$ 0.4 and $n = 2$ compare to the ratios β of other forces/moments within all cases. The ratio $\beta > 1$ for the moment M_n decreases as n decreases (Figures 4a-4b). The ratio $\beta > 1$ for the moment M_b increases as ξ decreases (Figures 5a-5b) or n decreases (Figures 5c-5d).

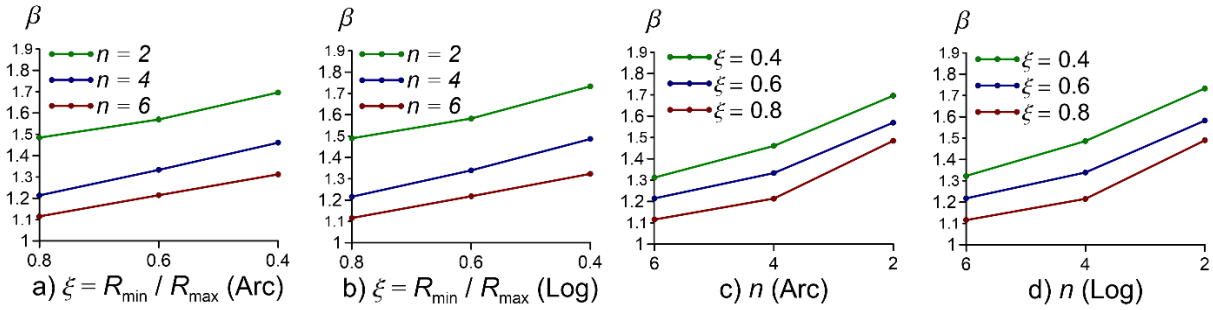

Figure 1. The ratio β for the force T_t of both exact conical helices. (Arc: Archimedean, Log: logarithmic).

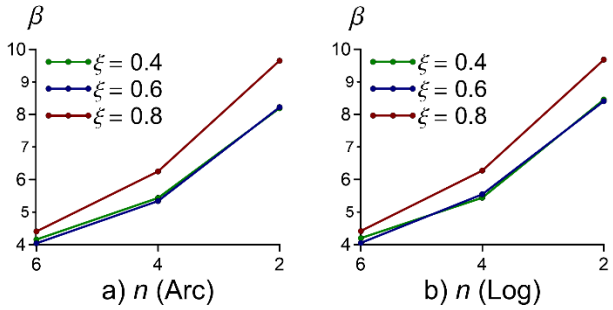

Figure 2. The ratio β for the force T_n of both exact conical helices. (Arc: Archimedean, Log: logarithmic).

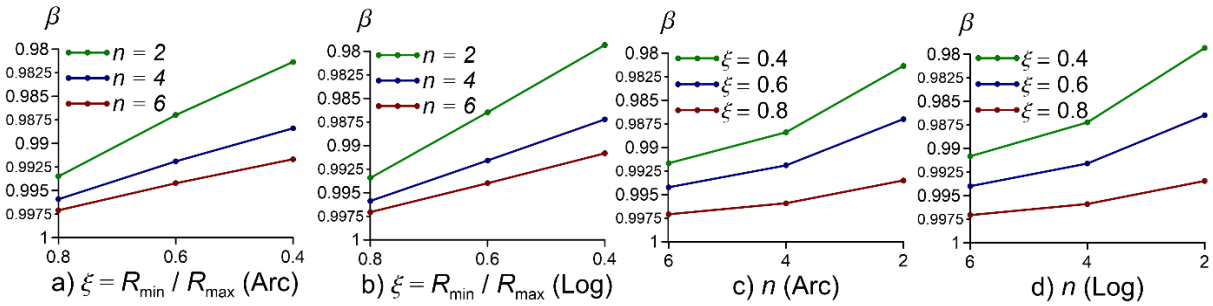

Figure 3. The ratio β for the force T_b of both exact conical helices. (Arc: Archimedean, Log: logarithmic).

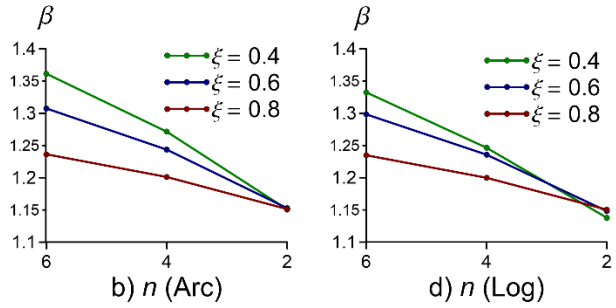

Figure 4. The ratio β for the force M_n of both exact conical helices. (Arc: Archimedean, Log: logarithmic).

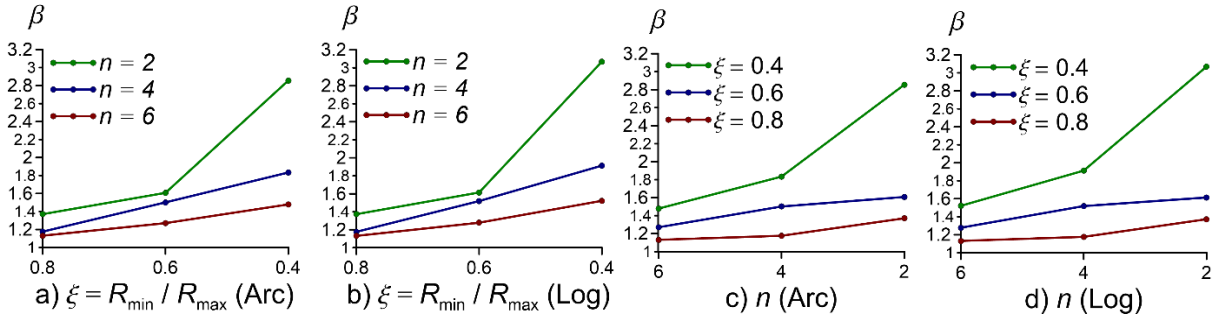

Figure 5. The ratio β for the force M_b of both exact conical helices. (Arc: Archimedean, Log: logarithmic).

4. Conclusions

The influence of warping of cross-section on the precision of forces and moments of exact conical helices is investigated using the mixed finite element formulation. The function of the exact axial geometry of conical helices given in Ermis and Omurtag (2017) is used. The inclusion procedure of the numerically determined warping considered torsional rigidity of rectangular sandwich sections is given in Aribas et al. (2019).

The ratio of warping included forces to the forces obtained disregarding the warping $\beta > 1$ increases as the number of the active turns n decreases for the forces T_t and T_n. It increases up to ~9.68 as n decreases for T_n. The maximum ratio $\beta \cong 9.68$ is obtained for T_n, $\xi = 0.8$ and $n = 2$. The ratio $\beta > 1$ increases as ξ decreases for the force T_t. However, the ratio $\beta < 1$ decreases as ξ decreases for the force T_b. The minimum ratio $\beta \cong 0.98$ is obtained for T_b, $\xi = 0.4$ and $n = 2$. The ratio $\beta > 1$ of the warping included moments to the moments obtained disregarding the warping decreases as n decreases for the moment M_n. However, the ratio $\beta > 1$ increases up to ~3.07 as n decreases for the moment M_b. The influence of cross-sectional warping on the precision of forces/moments is greater for the exact conical helix over logarithmic planar curve except the moment M_n compare to the exact conical helix over Archimedean planar curve.

References

Abramovich, H., Livshits, A. (1994). Free vibrations of non-symmetric cross-ply laminated composite beams. *Journal of Sound and Vibration*, 176: 597–612. https://doi.org/10/dmtf47

Aguiar, R.M., Moleiro, F., Mota Soares, C.M. (2012). Assessment of mixed and displacement-based models for static analysis of composite beams of different cross-sections. *Composite Structures*, 94: 601–616. https://doi.org/10/drqjtb

Aribas, U.N., Ermis, M., Eratli, N., Omurtag, M.H. (2019). The static and dynamic analyses of warping included composite exact conical helix by mixed FEM. *Composites Part B: Engineering*, 160: 285–297. https://doi.org/10/gft72h

Aydogdu, M. (2005). Vibration analysis of cross-ply laminated beams with general boundary conditions by Ritz method. *International Journal of Mechanical Sciences*, 47: 1740–1755. https://doi.org/10/bxhzvc
Babuska, P., Wiebe, R., Motley, M.R. (2018). A beam finite element for analysis of composite beams with the inclusion of bend-twist coupling. *Composite Structures*, 189: 707–717. https://doi.org/10/gc9rf7
Barretta, R. (2012). On the relative position of twist and shear centres in the orthotropic and fiberwise homogeneous Saint–Venant beam theory. *International Journal of Solids and Structures*, 49: 3038–3046. https://doi.org/10/f385gf
Bhimaraddi, A., Chandrashekhara, K. (1991). Some observations on the modeling of laminated composite beams with general lay-ups. *Composite Structures*, 19: 371–380. https://doi.org/10/fjj4db
Çalım, F.F. (2009). Dynamic analysis of composite coil springs of arbitrary shape. *Composites Part B: Engineering*, 40: 741–757. https://doi.org/10/cz26s7
Carpentieri, G., Tornabene, F., Ascione, L., Fraternali, F. (2015). An accurate one-dimensional theory for the dynamics of laminated composite curved beams. *Journal of Sound and Vibration*, 336: 96–105. https://doi.org/10/gddhkd
Darılmaz, K., Orakdöğen, E., Girgin, K. (2018). Saint-Venant torsion of arbitrarily shaped orthotropic composite or FGM sections by a hybrid finite element approach. *Acta Mech*, 229: 1387–1398. https://doi.org/10/gc6xzg
El Fatmi, R., Ghazouani, N. (2011). Higher order composite beam theory built on Saint-Venant's solution. Part-I: Theoretical developments. *Composite Structures*, 93: 557–566. https://doi.org/10/b35hv7
El Fatmi, R., Zenzri, H. (2004). A numerical method for the exact elastic beam theory. Applications to homogeneous and composite beams. *International Journal of Solids and Structures*, 41: 2521–2537. https://doi.org/10/b46zq6
Ermis, M., Omurtag, M.H. (2017). Static and dynamic analysis of conical helices based on exact geometry via mixed FEM. *International Journal of Mechanical Sciences*, 131–132: 296–304. https://doi.org/10/gcf8rr
Hu, M.Z., Kolsky, H., Pipkin, A.C. (1985). Bending Theory for Fiber-Reinforced Beams. *Journal of Composite Materials*, 19: 235–249. https://doi.org/10/cpzvgq
Jog, C.S., Mokashi, I.S. (2014). A finite element method for the Saint-Venant torsion and bending problems for prismatic beams. *Computers & Structures*, 135: 62–72. https://doi.org/10/gc6xzc
Jones, R.M. (1999). Mechanics of composite materials, 2nd ed., Taylor & Francis, Philadelphia, PA.
Jun, L., Hongxing, H., Rongying, S. (2008). Dynamic finite element method for generally laminated composite beams. *International Journal of Mechanical Sciences*, 50: 466–480. https://doi.org/10/fn9dxh
Kapania, R.K., Raciti, S. (1989). Recent advances in analysis of laminated beams and plates. Part I - Shear effects and buckling. *AIAA Journal*, 27: 923–935.
Kennedy, G.J., Hansen, J.S., Martins, J.R.R.A. (2011). A Timoshenko beam theory with pressure corrections for layered orthotropic beams. *International Journal of Solids and Structures*, 48: 2373–2382. https://doi.org/10/b3gtk7
Khdeir, A.A., Reddy, J.N. (1997). An exact solution for the bending of thin and thick cross-ply laminated beams. *Composite Structures*, 37: 195–203. https://doi.org/10/dbvxwp
Krishnaswamy, S., Chandrashekhara, K., Wu, W.Z.B. (1992). Analytical solutions to vibration of generally layered composite beams. *Journal of Sound and Vibration*, 159: 85–99. https://doi.org/10/cwfqz6
Nguyen, N.-D., Nguyen, T.-K., Thai, H.-T., Vo, T.P. (2018). A Ritz type solution with exponential trial functions for laminated composite beams based on the modified couple stress theory. *Composite Structures*, 191: 154–167. https://doi.org/10/gc9rch
Nguyen, T.-K., Nguyen, N.-D., Vo, T.P., Thai, H.-T. (2017). Trigonometric-series solution for analysis of laminated composite beams. *Composite Structures*, 160: 142–151. https://doi.org/10/f9hqdc
Nouri, T., Gay, D. (1994). Shear stresses in orthotropic composite beams. *International Journal of Engineering Science*, 32: 1647–1667. https://doi.org/10/fkhsbm
Oden, J.T., Reddy, J.N. (2012). Variational methods in theoretical mechanics. Springer Science & Business Media.
Omurtag, M.H., Aköz, A.Y. (1994). Hyperbolic paraboloid shell analysis via mixed finite element formulation. *International Journal for Numerical Methods in Engineering*, 37: 3037–3056. https://doi.org/10/fw3r2c
Omurtag, M.H., Aköz, A.Y. (1992). The mixed finite element solution of helical beams with variable cross-section under arbitrary loading. *Computers & Structures*, 43: 325–331. https://doi.org/10/b644p8
Savoia, M., Tullini, N. (1993). Torsional response of inhomogeneous and multilayered composite beams. *Composite Structures*, 25: 587–594. https://doi.org/10/c3v6hx
Swanson, S.R. (1998). Torsion of laminated rectangular rods. *Composite Structures*, 42: 23–31. https://doi.org/10/b6r8fn
Temel, B., Çalım, F.F., Tütüncü, N. (2005). Forced vibration of composite cylindrical helical rods. *International Journal of Mechanical Sciences*, 47: 998–1022. https://doi.org/10/cgwfzd
Vo, T.P., Thai, H.-T. (2012). Static behavior of composite beams using various refined shear deformation theories. *Composite Structures*, 94: 2513–2522. https://doi.org/10/f32hbn

Yan, Y., Pagani, A., Carrera, E. (2017). Exact solutions for free vibration analysis of laminated, box and sandwich beams by refined layer-wise theory. *Composite Structures*, 175: 28–45. https://doi.org/10/gddhkc

Yıldırım, V. (1999). Governing equations of initially twisted elastic space rods made of laminated composite materials. *International Journal of Engineering Science*, 37: 1007–1035. https://doi.org/10/d384x5

Yıldırım, V., Sancaktar, E. (2000). Linear free vibration analysis of cross-ply laminated cylindrical helical springs. *International Journal of Mechanical Sciences*, 42: 1153–1169. https://doi.org/10/fjkh5z

Yousefi, A., Rastgoo, A. (2011). Free vibration of functionally graded spatial curved beams. *Composite Structures*, 93: 3048–3056. https://doi.org/10/fv78qz

Yu, A., Hao, Y. (2013). Effect of warping on natural frequencies of symmetrical cross-ply laminated composite non-cylindrical helical springs. *International Journal of Mechanical Sciences*, 74: 65–72. https://doi.org/10/f46vnq